Molecular Therapy
Methods & Clinical Development
Original Article

Predictive power of deleterious single amino acid changes to infer on AAV2 and AAV2-13 capsids fitness

Tiziana La Bella,[1,2,6] Bérangère Bertin,[1,2] Ante Mihaljevic,[1,2] Justine Nozi,[1,2] Patrice Vidal,[1,2] Sandrine Imbeaud,[3] Jean-Charles Nault,[3,4] Jessica Zucman-Rossi,[3,5] and Giuseppe Ronzitti[1,2,6]

[1]Genethon, 91000 Evry, France; [2]Université Paris-Saclay, University Evry, Inserm, Genethon, Integrare Research Unit UMR_S951, 91000 Evry, France; [3]Centre de Recherche des Cordeliers, Sorbonne Université, Université de Paris, INSERM, 75000 Paris, France; [4]Avicenne Hospital, Paris-Seine-Saint-Denis University Hospital, APHP, 93000 Bobigny, France; [5]Hôpital Européen Georges Pompidou, AP-HP, 75000 Paris, France

Adeno-associated virus (AAV) is the most widely used vector for *in vivo* gene transfer. A major limitation of capsid engineering is the incomplete understanding of the consequences of multiple amino acid variations on AAV capsid stability resulting in high frequency of non-viable capsids. In this context, the study of natural AAV variants can provide valuable insights into capsid regions that exhibit greater tolerance to mutations. Here, the characterization of AAV2 variants and the analysis of two public capsid libraries highlighted common features associated with deleterious mutations, suggesting that the impact of mutations on capsid viability is strictly dependent on their 3D location within the capsid structure. We developed a novel prediction method to infer the fitness of AAV2 variants containing multiple amino acid variations with 98% sensitivity, 98% accuracy, and 95% specificity. This novel approach might streamline the development of AAV vector libraries enriched in viable capsids, thus accelerating the identification of therapeutic candidates among engineered capsids.

INTRODUCTION

Adeno-associated virus (AAV) is a small non-enveloped virus belonging to the *Dependoparvovirus* genus within the *Parvoviridae* family.[1] AAV is naturally replication defective, meaning that it requires a helper virus, such as adenovirus or herpes virus, to complete its life cycle. The genome consists of a single-stranded DNA molecule of about 4.7 kilobases in length. It has two open reading frames, one encoding the viral capsid proteins (VP1, VP2, and VP3) and the other encoding regulatory and replication proteins (Rep78, Rep68, Rep52, and Rep40).[2] In addition, three accessory proteins, MAAP (membrane-associated accessory protein), AAP (assembly-activating protein), and X, are expressed from frameshifted open reading frames within the capsid genes.[3–6] The viral capsid proteins assemble into a protein shell that surrounds and protects the viral genome and that determines the virus tropism by interacting with specific cell receptors and co-receptors on the target organ. Tissue tropism is directly linked to the sequence and conformation of the looped-out domains of VP proteins that compose the capsid. Noteworthy, the amino acid variability of the VP sequence of different AAV serotypes cluster in 12 hypervariable regions (HVRs), which mainly correspond to the looped-out domains.[7]

AAV is highly attractive as a gene therapy vector due to its low immunogenicity and low pathogenicity, its ability to infect both dividing and non-dividing cells, and its persistence as transcriptionally active episome, allowing for long-term expression of the therapeutic gene.[8,9] The exponential growth of clinical trials using AAV reflects the enormous potential of this system in various therapeutic areas.[10] One of the key advantages of AAV vectors is the high versatility due to the large number of wild-type (WT) and engineered capsid variants, each characterized by specific tissue tropism. To date, 13 distinct serotypes and more than 100 WT variants have been isolated from natural sources, among which AAV2 is the most frequently isolated serotype in human.[11–15]

AAV capsid engineering is based on the modification of the capsid protein sequence to improve various characteristics such as productivity, biodistribution or to reduce immunogenicity.[16–19] Different methods exist to modify the capsid structure.[20] Among these, directed evolution relies on the generation of a library of millions of variants followed by multiple selection steps allowing to retrieve the best candidates. One of the major issues related to this approach is the high frequency of non-viable capsids.[4,21,22] The incomplete understanding of the consequences of amino acid variations on capsid stability still poses a major problem in capsid engineering. Given the extensive knowledge available on the structure-function relationship in AAV2 vector mutants, WT capsid variants of the AAV2 serotype represent a unique opportunity to study the impact of multiple mutations on the stability of the AAV capsid to identify regions that

Received 4 April 2024; accepted 15 August 2024;
https://doi.org/10.1016/j.omtm.2024.101327.

[6]These authors contributed equally

corresponding author: Giuseppe Ronzitti, Genethon, 91000 Evry, France.
E-mail: gronzitti@genethon.fr

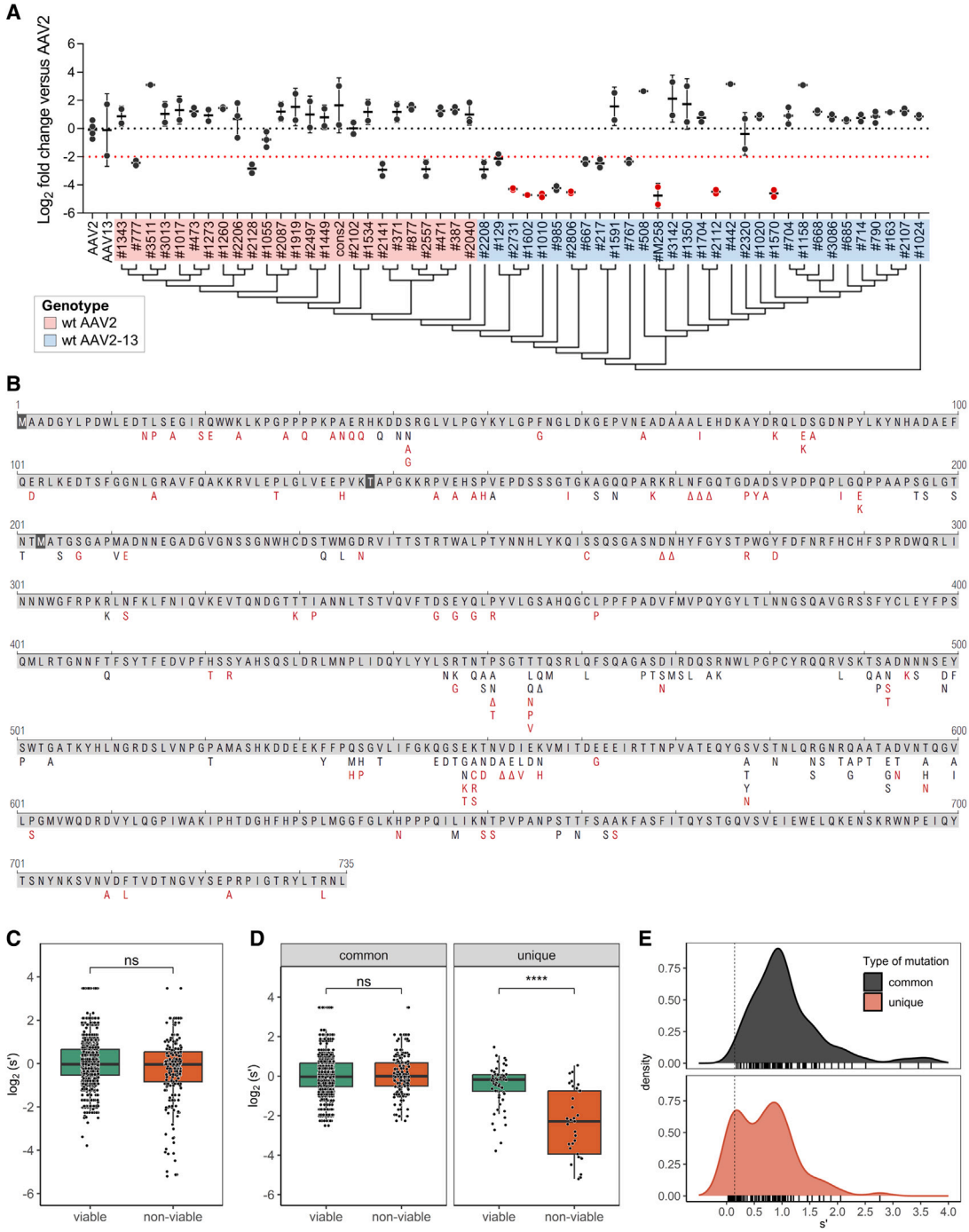

Figure 1. Manufacturability and mutations landscape of WT AAV variants

(A) Production of AAV variants in 50 mL of HEK293T cells growing in suspension. Titers of production are expressed as vector genomes per mL (vg/mL) and normalized as fold change compared with the AAV2 control capsid. Each variant was independently produced twice. The mean value of the titers and SD are indicated per each variant. Black and red dotted lines represent the level of AAV2 production and the production threshold, respectively. Variants labeled in red are characterized by large indels or frameshift mutations. Phylogenetic tree on VP1 coding protein region of WT AAV variants is represented on the bottom. The tree was constructed using the neighbor joining method[27] based on the evolutionary distances computed by the Poisson correction method.[28] The representation is toggled for topology scale. (B) Landscape of mutations identified in WT AAV variants. AAV2 sequence is used as reference, common (black) and unique (red) mutations are listed below each position. The start codons of VP proteins are highlighted in dark gray. Variants with indels and frameshift mutations are not represented. (C) Median viability s' score for all mutations belonging to viable ($n = 40$)

(legend continued on next page)

most tolerate mutations and streamline the development of novel capsids.

In 2020, we screened a cohort of 1,319 human liver tissues and isolated 59 new capsid variants equally distributed in two distinct subtypes: AAV2 and AAV2-13 hybrids.[23] In this study, AAV vectors derived from these novel AAVs were characterized in terms of manufacturability and transduction efficiency. AAV viability was correlated to capsid mutations to identify common features among non-viable variants. We then took advantage of the recently published AAV2 capsid fitness landscape,[4] describing the effects of single point mutations on capsid production. In this study, Ogden and colleagues transfected a plasmid library, including all possible single-codon substitutions, insertions, and deletions over the entire VP sequence, in HEK293T cells to produce recombinant AAV virus. They computed the fitness of each variant, expressed as the mutant frequency in the virus pool divided by its frequency in the plasmid pool, and normalized this selection value (s) as enrichment relative to AAV2 capsid (s'). In this work, we used the s' score associated to single point mutations to develop a method for predicting the collective impact of multiple mutations on AAV vector viability. This approach relies on the hypothesis of mutation independence, which implies that capsid viability is not determined by the cumulative impact of all mutations present in the VP, but rather due to the independent effect of each mutation. Consequently, the presence of a single deleterious mutation can be sufficient to irreversibly impair capsid fitness. Our method, validated across multiple collections of mutated AAV2 capsids, allows to infer the fitness of variants with multiple amino acid variations, providing a useful tool to guide the design of engineered capsids.

RESULTS

Manufacturability of AAV vectors derived from novel AAV variants

The series of 59 capsid variants, consisting of 25 AAV2 and 34 AAV2-13 variants,[23] was used to derive the consensus sequences corresponding to the two AAV genotypes. A pairwise analysis (Table S1) was performed to exclude redundant amino acid sequences from the capsids collection resulting in a final list of 56 capsids. The list comprises 24 AAV2 and 31 AAV2-13 sequences, and the consensus sequence of all AAV2 variants. The VP sequences were cloned into a vector suitable for AAV vector production to assess the capsid viability. All capsids with a production yield equal to or higher than 1.5×10^{10} vg/mL and the ability to transduce 2V6.11 cells were considered as viable (Figure S1A). 2V6.11 cells are genetically modified HEK293T cells that express the adenovirus E4 ORF gene upon induction, which renders these cells highly permissive to AAV infection.[24]

In total, 39 out of 56 AAV variants were successfully produced (Figure 1A). For 37 capsids, production yields of AAV vectors were either comparable with or higher than AAV2 (5.9×10^{10} vg/mL). In addition, all produced variants were able to transduce cells *in vitro* (Figure S1B). To verify the non-viability of the 17 variants with low production yields, bulk vectors were used to transduce 2V6.11 cells (Figure S1C). Among the 17 variants tested, 16 displayed transduction efficiency either below or close to the negative control, whereas #129 variant reached the transduction level of AAV8, a capsid known for its poor *in vitro* transduction efficacy.[25] Considering that the productivity of this variant was at the threshold limit (1.4×10^{10} vg/mL) and that it showed some transduction activity before vector purification, #129 was classified as a viable capsid, although it presented some manufacturability issues. Interestingly, 53 out of 56 capsid variants had mutations in the arginine residues at positions 585 and/or 588 (Table S2), which are crucial for AAV2 binding to the heparan sulfate proteoglycan (HSPG) receptor, a primary AAV2 receptor responsible for its high *in vitro* transduction efficiency.[26] Capsid variant #129 was the only viable variant that retained binding to the HSPG receptor, which may explain why we were able to detect transduction activity with low titer of #129 bulk vector. In total, 40 out of 56 variants met our viability criteria, including 21 out of 25 AAV2 and 19 out of 31 AAV2-13 sequences.

AAV production was correlated to mutations in structural and non-structural proteins to identify common features among the 16 non-viable capsids. Indels with sizes ranging from 24 to 72 nucleotides likely explained the non-viability of 6 variants (#1010, #2731, #1602, #2806, #2112, and #1570), as well as a 156-nt frameshift mutation in one variant (#M258; Figure S1D). These mutations were not localized within a specific hotspot in VP sequence, but rather affected a significant portion of the VP protein structure, including the β sheet regions. Since those 7 variants were AAV2-13, we compared the impact of the peptide insertion or frameshift mutations on AAV13 reference capsid (GenBank: ABZ10812.1), which shares 93% sequence homology. The GRAVY (Grand Average of Hydropathy) index, defined as the average hydropathy value of a peptide or protein,[29] was calculated for the impacted VP region in AAV13 and for mutant peptides to evaluate possible variations in hydrophobicity (Figure S2A). The nature of the impacted VP regions was predominantly hydrophilic, and the mutations mainly induced an increase in hydrophobicity (in four out of seven variants), which may contribute to the destabilization the capsid structure. To confirm destabilization, the VP3 3D structures of those variants were modeled using an AlphaFold2-based algorithm (Figures S2B–S2F) and superimposed to AAV13 (PDB: 7L6H) underlining the presence of conformational change in the mutated regions. The root mean-square deviation (RMSD), which quantifies the average distance between the

and non-viable capsids ($n = 9$). Statistical analysis was performed using Wilcoxon rank-sum test. (D) Median viability s' score for common and unique mutations belonging to viable ($n = 40$) and non-viable capsids ($n = 9$). Statistical analysis was performed using Wilcoxon rank-sum test. (E) Frequency distribution represented as density of the s' scores of common and unique mutations in WT AAV variants. Rug plot below each density plot shows the distribution of s' data. The vertical dashed line represents the threshold of potentially deleterious mutations. Mutations with s' > 4 are not represented in the graph. $^{*}p < 0.05$, $^{**}p < 0.01$, $^{***}p < 0.001$, $^{****}p < 0.0001$.

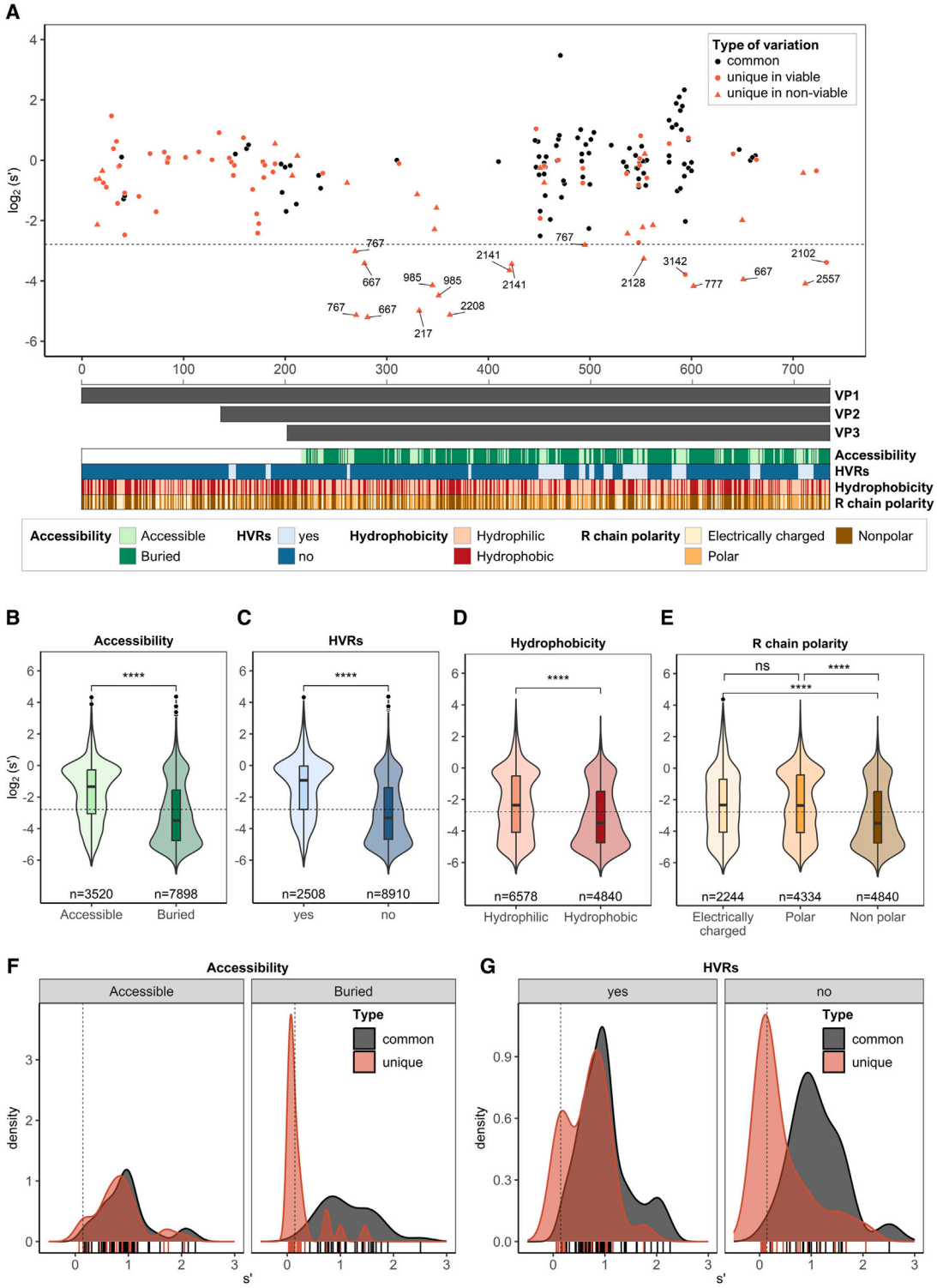

Figure 2. Representative features of deleterious mutations

(A) Scatter plot showing the s' scores associated to all mutations in WT AAV variants along the VP sequence. Mutations are categorized in common (black) and unique (red) variations. Unique mutations belonging to non-viable capsids are represented as triangles. Mutations below the s' threshold (horizontal dashed line) are labeled with the names of the corresponding AAV variants. VP positions and major amino acid features (residue accessibility, HVRs position, hydrophobicity, and polarity of the amino acids)

(legend continued on next page)

atoms of superimposed proteins, was calculated. The VP protein models displayed an overall high structure homology to AAV13 (Figure S2G) with the exception of #M258, characterized by an RMSD of 8.58 Å. VP structures of #2731 and #1602 were not predicted because the indels were located in regions outside the crystallized sequence of AAV13 VP3.

The sequence analysis of accessory proteins in both viable and non-viable variants did not reveal any common variation in AAP, MAAP, and X proteins unique to non-viable capsids (Figure S1A). The sole exception was the presence of premature stop codons in AAP protein (Figures S1A and S1D) caused by the indels in #1010, #2731, and #1602, and the frameshift mutation in #M258, which might have also negatively impacted the production of these capsids.

Concerning the analysis of structural protein sequences, no recurrent amino acid variations or mutation hotspots were identified within the VP of non-viable capsids. In conclusion, while we gained some insights into the lack of viability for 7 out of the 16 non-viable capsids, the remaining 9 AAV variants had only point mutations compared with AAV2, and there was no apparent cause for their lack of viability.

Independent contribution of single mutations in predicting capsid viability

To ensure an unbiased examination of the impact of single mutations on AAV capsid viability, previously described variants with indels and frameshift mutations were excluded from the subsequent analysis. Among the remaining 49 AAV capsid variants, comprising 40 viable and 9 non-viable ones, a total of 183 single mutations (Figure 1B; Table S3) were identified when compared with AAV2 reference (GenBank: YP_680426.1). These mutations encompassed 174 substitutions and 9 deletions distributed across the entire VP sequence. We integrated the publicly available dataset from Ogden and colleagues[4] and associated the fitness score (s'), calculated for the single amino acid variations, to each mutation present in our variants. Although the s' scores were similar for viable and non-viable capsids (Figure 1C), non-viable variants showed an enrichment in mutations with a lower s' score compared with viable variants.

Point mutations were then classified based on their frequency in our series in two categories: common mutations (n = 90), present in at least two AAV capsid variants, and unique mutations (n = 93), present only in one capsid variant (Figure 1B; Table S3). When common mutations were considered (Figure 1D, left panel), no differences in the s' score were found between viable and non-viable capsids, whereas unique mutations (Figure 1D, right panel) had a significant 4-fold reduction in s' in non-viable capsids. The s' score for common mutations (Figures 1E and S3A) ranged from 11.1 to 0.18 and was normally distributed (p = 0.99, Hartigan's dip test) with a peak at 0.91. Conversely, in unique mutations (Figures 1E and S3A) the s' ranged from 2.76 to 0.03 and displayed a bimodal distribution (p = 0.047, Hartigan's dip test) with a first peak at 0.96, similar to that seen in common mutations, and a lower peak at 0.14. We set an arbitrary s' threshold for deleterious mutations at 0.145, positioned right after the peak observed in potentially deleterious unique mutations (0.14) and before the s' range associated with common mutations.

We used this threshold to predict the viability of our variants based on the hypothesis that the viability is affected by the presence of individual mutations with a low s' score. This hypothesis of mutation independence was clearly exemplified by two WT variants, the non-viable capsid #777 and the viable capsid #1343, which VP sequences only differed by one amino acid (P602S, s' = 0.055). We consider this variation, predicted as deleterious in #777, as responsible for the loss of viability of the variant.

We inferred the viability of the 49 variants according to the independent contribution of single mutations and found that 47 out of 49 capsids were correctly predicted (Figure 2A). All non-viable capsids harbored at least one or multiple unique deleterious mutations distributed between position 269 and the end of the VP. Interestingly, none of the 15 potentially deleterious mutations identified in non-viable variants was present in any other analyzed AAV serotypes (Table S4), suggesting that those mutations might be deleterious regardless of the AAV serotype. Moreover, the presence of common or unique mutations with a high s' score in these variants was unable to rescue the impairment caused by deleterious mutations suggesting that a compensatory effect is unlikely (Figures 2A and S3B). Among the 40 viable AAV capsids, 38 did not contain any unique point mutations with an s' score below 0.145. Two exceptions were present in our series (Figures 2A and S3C–S3E): the viable capsids #2102 and #3142, both having single unique mutations below the threshold and consequently predicted as non-viable. By correlating the production yields with the minimum s' score for each variant (Figures S3C–S3E), we were able to unequivocally highlight the two outliers in our prediction method, as well as the viable variant with poor manufacturability (#129). The analysis was reliable only when unique mutations were included in the correlation. Concerning the viable variant #2102, a potential deleterious mutation R733L with an s' value of 0.095 led to its classification as a non-viable capsid. Due to the localization at the very end of the VP3 sequence, we hypothesized that mutations in this region might have a lower impact on capsid structure and viability. Similarly, mutation D594N (s' = 0.072) identified in the viable variant #3142, was localized in a region known to tolerate

are represented below the graph. (B) Median s' scores of mutations in Ogden and colleagues' dataset[4] according to the accessibility of the residues, (C) localization within or outside HVRs, (D) hydrophobicity of the mutated amino acid, and (E) polarity of the R chain of the mutated residue. Median, interquartile range, minimum, and maximum values are represented in the boxplot. The violin plot shows the distribution of the data points. Outliers are indicated as individual dots. Statistical analysis was performed using Wilcoxon rank-sum test. (F) Density distribution of s' scores of mutations in WT AAVs according to the accessibility of the residues, and (G) the localization within or outside the HVRs. The s' score distributions of common and unique mutations are shown according to analyzed features. Rug plot below each density plot shows the distribution of s' data. The vertical dashed line represents the threshold of potentially deleterious mutations. *p < 0.05, **p < 0.01, ***p < 0.001, ****p < 0.0001.

capsid variation, the HVR10, also known as VR-VIII.[7] Notably, HVR10 is one of the most frequently used sites for peptide insertion,[30–32] moreover asparagine residues at position 594 are also found in AAV10, AAV11, and AAV12 (Table S4).

Relevant capsid features for viability prediction

To identify common amino acid features strictly linked to viability prediction, we focused on four major parameters: accessibility in the 3D capsid structure, localization within HVRs,[7] hydrophobicity, and polarity of mutated amino acid (Figure 2A, bottom panel). For the two parameters related to the residue position (accessibility and HVR), our analysis was restricted to the crystalized capsid region, excluding the first 216 residues of the VP.

To retrieve the capsid accessibility of amino acid residues, we first compared the crystal structures of AAV2 (PDB: 1LP3) and AAV13 (PDB: 7L6H). The crystallized VP protein sequence of AAV2 shared 99% and 89% homology with the consensus sequences of WT AAV2 variants and WT AAV2-13 variants, respectively. On the contrary, the crystal structure of AAV13 showed 97% homology with the consensus sequence of AAV2-13, suggesting that it might be more suitable for predicting AAV2-13 accessibility. However, the superposition of AAV2 and AAV13 VP monomers (Figure S4A) showed a high structure homology, with an RMSD of only 0.65 Å. In addition, the accessible surface percentages of amino acid residues within AAV2 and AAV13 capsids was well correlated over the entire length of the VP protein (Figures S4B and S4C), therefore we decided to use the 3D structure of AAV2 for our further analyses.

First, the s' score of single amino acid variations in Ogden and colleagues' series[4] was analyzed across multiple parameters related to AAV2 3D structure and sequence to pinpoint the most relevant features. We observed an important effect of residue accessibility on the s' score (Figure 2B). Specifically, mutations in buried residues displayed a median s' value of 0.089, which was significantly (4-fold) lower than the median s' (0.395) of mutations in accessible residues. Similarly, a 5-fold reduction in s' value was associated with mutations in residues located outside HVRs compared with those within HVRs (0.523 and 0.100, respectively; Figure 2C). Concerning the type of amino acid side chain (Figure 2D), s' score was significantly decreased (2-fold) for mutations of amino acids with hydrophobic side chains compared with those with hydrophilic side chains (0.088 and 0.194, respectively). Furthermore, mutations of amino acids with electrically charged and polar side chains (Figure 2E) exhibited similar mean s' values (0.198 and 0.194), whereas mutations of nonpolar amino acids resulted in significantly lower s' value (0.088).

In our collection of capsid variants, common mutations did not show any significant variation according to the analyzed parameters (Figures S5A–S5D), s' score was stable at 0.90–0.98. On the contrary, a significantly lower s' value was associated with unique mutations in buried residues (s' = 0.096; Figure S5A) that displayed a 9-fold decreased s' score compared with mutations in accessible residues (s' = 0.833). Notably, the s' distribution of common and unique mutations (Figure 2F, left panel) showed an overlapping Gaussian distribution within accessible residues ($p = 0.99$ and $p = 0.57$ for common and unique mutations, respectively, Hartigan's dip test). In contrast, buried residues (Figure 2F, right panel) had a completely different distribution with unique mutations clustering in a unique peak below the s' threshold of 0.145 ($p = 0.89$, Hartigan's dip test). Common mutations in buried residues also followed a normal distribution ($p = 0.89$, Hartigan's dip test), with a peak at s' = 0.85.

Similarly, the median s' value of unique mutations outside HVRs (Figure S5B) was 4-fold lower than that observed in residues within HRVs (0.164 and 0.735, respectively). The s' distribution of unique mutations within HVRs (Figure 2G, left panel) was bimodal ($p = 0.048$, Hartigan's dip test) with a peak overlapping the unimodal distribution of the common mutations ($p = 1$, Hartigan's dip test) and a specific peak corresponding to the s' threshold. Conversely, for residues outside HVRs (Figure 2G, right panel), both unique and common mutations displayed a unimodal s' distribution ($p = 0.93$ and $p = 0.87$, Hartigan's dip test), with the peak of unique mutations aligning with the s' threshold. Concerning the features related to the nature of the mutated amino acids (Figures S5C and S5D), no significant differences were observed in unique mutations according to the hydrophobicity and polarity of the mutated residues.

We then explored the effect of amino acid variations according to the type of mutations. We classified the mutations from Ogden and colleagues' dataset according to our own s' threshold into two categories: neutral and deleterious. First, we focused on assessing the change in amino acid hydrophobicity, and we looked at the frequency of each type of alteration (Figures S6A–S6D). Mutations involving the change from hydrophobic residue to a hydrophilic one, as well as deletions and stop codon insertions, were more frequently deleterious than neutral. Subsequently, we examined the effect of amino acid variations according to capsid accessibility. Stop codon mutations were excluded from this analysis because they were predominantly deleterious across all residues along the VP sequence (Figure S6E). In accessible residues (Figure 3A, left panel), hydrophobic to hydrophilic mutations were more frequently deleterious than neutral (19% and 13%, respectively), whereas hydrophilic to hydrophilic mutations were more frequently neutral than deleterious (42% versus 28%, respectively). In buried residues (Figure 3A, right panel), most of the deleterious alterations were found to be hydrophobic to hydrophilic changes (32%) and their frequency was significantly higher compared with neural alterations (17%). All the other mutations were less frequently deleterious in buried regions. Deletions were more frequently deleterious in both accessible and buried residues regardless of the polarity of the deleted amino acid.

When analyzing the s' score according to the change in hydrophobicity of the mutated amino acid (Figure 3B), we observed that s' values were significantly lower in buried residues than in accessible ones for all types of alterations, except for stop codon mutations, which were always deleterious. Potentially deleterious mutations identified within

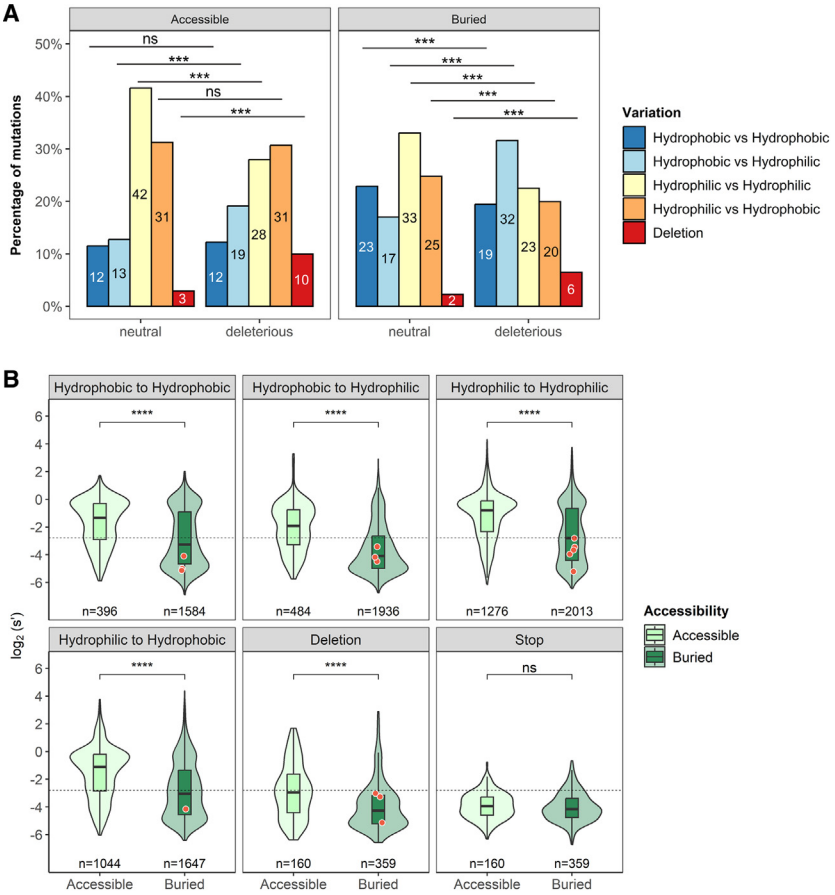

Figure 3. Type of amino acid change and impact on capsid viability according to residue accessibility

(A) Analysis of the major type of amino acid changes (variation in hydrophobicity) and deletions in accessible and buried residues. Mutations in the Ogden dataset were categorized in neutral and deleterious according to the s' value, then the frequency of the different types of variations was analyzed in each group. Statistical analysis was performed using χ^2 test with Monte Carlo simulation. (B) s' score of mutations in the Ogden dataset according to major hydrophobic changes, deletions, and stop codon integrations in accessible and buried residues. Median, interquartile range, minimum, and maximum values are represented in the boxplot. The violin plot shows the distribution of the data points. Potentially deleterious mutations identified in WT AAV variants are represented as individual red dots. Statistical analysis was performed using Wilcoxon rank-sum test. *$p < 0.05$, **$p < 0.01$, ***$p < 0.001$, ****$p < 0.0001$.

our cohort were all located in buried residues, but they were not enriched in a specific type of alteration.

We further analyzed the change in hydrophobicity of the residues according to the type of R chain in the mutated amino acid (Figures S7 and S8) and observed the same pattern with decreased s' score in buried residues compared with accessible ones across most variations. Notably, mutations involving transitions from one aromatic residue to another aromatic, from an acid to another acid, from an aromatic to an acid, and vice versa, showed similar s' score and distribution in both buried and accessible regions (Figures S7 and S8). Concerning potentially deleterious mutations identified in our cohort, no specific R chain variations were highlighted.

Taken together, the analysis of the mutations in Ogden and colleagues' series and in our collection of WT capsids collectively suggests that the 3D localization of residues, represented by their accessibility and in part by the HVR position, is the parameter that best identifies regions of AAV capsids where mutations are most likely deleterious. A multivariate analysis was performed to study the interaction of residue features in predicting neutral and deleterious mutations. In our dataset (Figure S9A), we found that the feature with the greatest impact on predicting neutral mutations was HVR localization (OR = 5.46, $p = 0.020$), followed by residue accessibility (OR = 1.12, $p = 0.007$), while hydrophilicity was not significantly associated with predicting neutral mutations (OR = 1.41, $p = 0.624$). Similarly, in Ogden and colleagues' series (Figure S9B), we observed that mutations in the HVR were strongly associated with an increased likelihood of being neutral (OR = 3.16, $p < 0.0001$). In addition, there was a slight but significant positive association between neutral mutations and both increased accessibility (OR = 1.03, $p < 0.0001$) and hydrophilicity of the amino acids (OR = 1.75, $p < 0.0001$). Overall, HVR localization and, to a lesser extent, residue accessibility were the parameters most strongly associated with predicting mutation outcomes in both Ogden and colleagues' dataset and our capsid collection. In line with this result, the simultaneous analysis of the residues' positions according to accessibility and HVRs localization in Ogden and colleagues' dataset (Figure 4A) revealed that the highest frequency of deleterious mutations was found in buried residues outside HVRs (65%), while the lowest frequency was observed in accessible residues within HVRs (15%). This finding was further validated in our own series (Figure 4B) where we observed that 12 out of 15 potentially deleterious mutations in non-viable capsids were located in buried regions outside HVRs, whereas only 3 mutations were in buried regions within HVRs. To further support this observation, the frequency of deleterious mutations along the VP sequences was compared with the frequency of accessible and buried residues, both within and outside HVRs (Figure 4C). The profile of potentially deleterious mutations mirrored the distribution of buried residues, more precisely buried residues outside HVRs, suggesting the interlink between these two variables.

Rescue of predicted deleterious residues further supports the independence of mutations

To prove that only the mutations below the s' threshold had affected the viability of the capsids, we performed reverse mutations of some

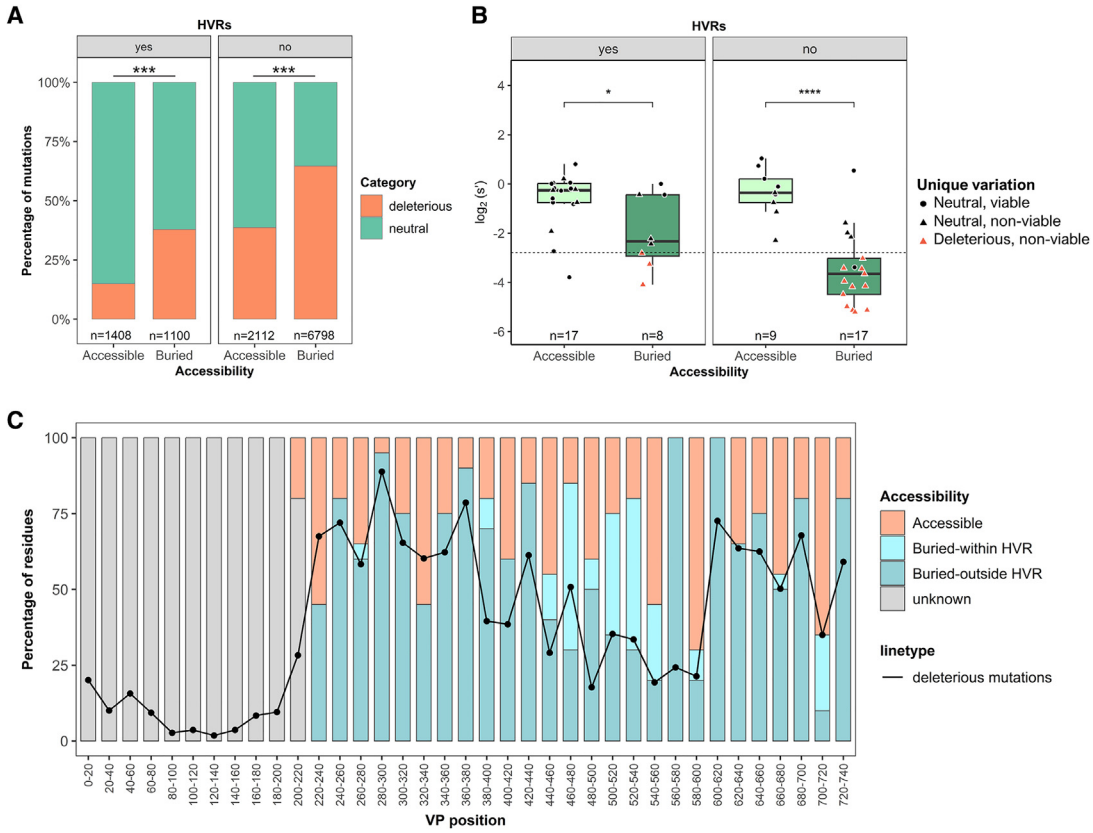

Figure 4. Interplay between accessibility and HVR localization in viability prediction

(A) Frequency of deleterious mutations in the Ogden dataset according to their localization in accessible and buried residues within or outside HVRs. Mutations were categorized in neutral and deleterious according to the s' value threshold. Statistical analysis was performed using χ^2 test with Monte Carlo simulation. (B) Median s' score of unique mutations of WT AAVs in accessible and buried residues within or outside HVRs. Median, interquartile range, minimum, and maximum values are represented in the boxplot. Horizontal dashed line represents the threshold of potentially deleterious mutations. Statistical analysis was performed using Wilcoxon rank-sum test. (C) Frequency of accessible and buried residues along the VP sequence calculated per window of 20 amino acids. Buried residues were divided in 2 groups: buried within HVR and buried outside HVR. The black line over the graph represents the frequency of deleterious mutations calculated in each 20 amino acid window. *$p < 0.05$, **$p < 0.01$, ***$p < 0.001$, ****$p < 0.0001$.

potentially deleterious mutations identified in our capsid variants. Common and unique mutations spanning a 256 amino acid region (AAV2 positions 350–606) from 3 WT variants, including 2 WT AAV2 (#2141 and #2128) and 1 WT AAV2-13 (#2208), were introduced in the AAV2 reference capsid (Figures 5A–5C). AAV vectors carrying a luciferase reporter gene were produced to assess both the manufacturability and transduction efficiency of the mutated capsids. The AAV2-2208 capsid (Figure 5A) contained 4 common mutations predicted as neutral and one potentially deleterious mutation (L362P, s' = 0.028). The reverse mutation of L362P successfully restored capsid viability, leading to an increase in both transducing titer and vector yields (Figures 5D and S10A). Similar positive outcomes were observed for capsid AAV2-2128 (Figure 5B), characterized by 3 common mutations and 3 unique mutations, one of which was predicted to be deleterious (D553del, s' = 0.104). The insertion of a D at position 553 induced the reversion of the phenotype with a noticeable increase of both luciferase activity and vector yields (Figures 5E and S10B). The last mutant capsid tested, AAV2-2141 (Figure 5C), presented 1 common and 3 unique mutations, 2 of which were potentially deleterious (H421T, s' = 0.079; and S423R, s' = 0.092). Importantly, only the double mutant led to the production of a viable capsid, whereas individual reversion of the single deleterious mutation was insufficient to recover infectivity or enhance vector yields (Figures 5F and S10C).

These results experimentally validated the prediction of the deleterious mutations using the s' score and the established threshold. Furthermore, these findings provide substantial support for our initial hypothesis regarding the independence of mutations, affirming that isolated mutations can indeed exert a deleterious effect on the overall capsid's structure and viability.

Validation of the prediction method in public datasets

To further validate our prediction method, we used publicly available data from two independent datasets. The first capsid library was generated by introducing random substitutions at five positions of

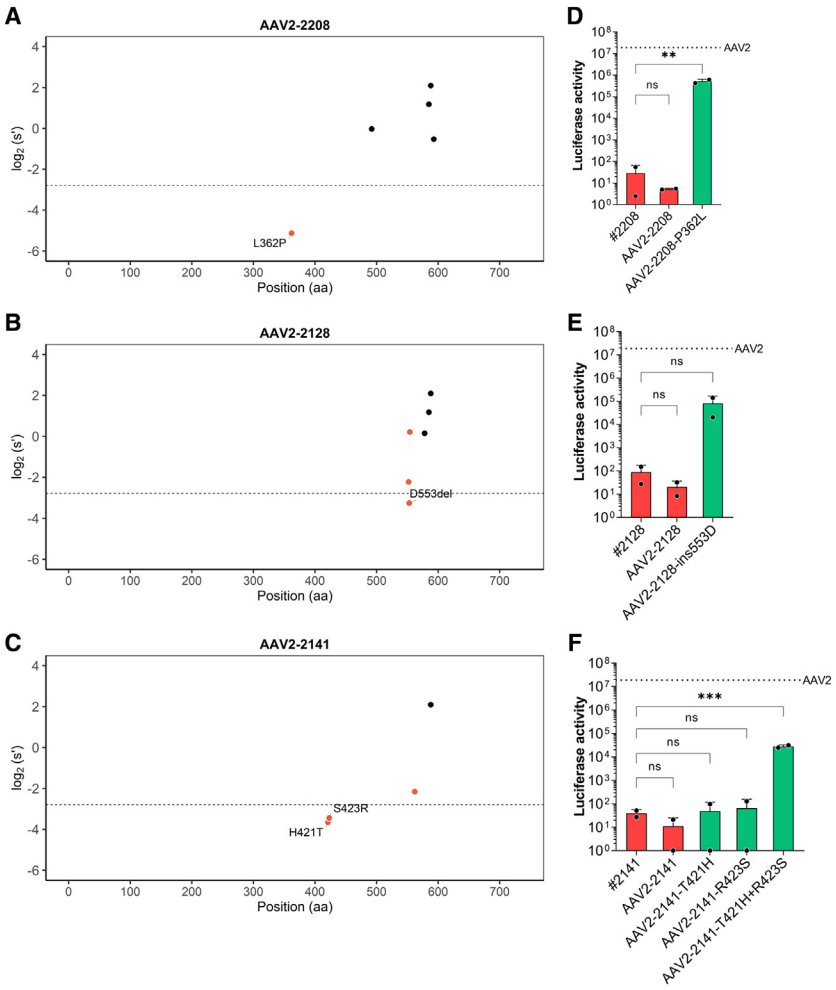

Figure 5. Experimental validation of potentially deleterious mutations on capsid viability

Schematic representation of common (black) and unique (red) mutations with associated s' score in VP sequence of hybrid capsids: (A) AAV2-2208, (B) AAV2-2128, and (C) AAV2-2141. Potentially deleterious mutations are represented below the s' threshold (horizontal dashed line) and labeled with the name of the corresponding variation. The impact of potentially deleterious mutations was evaluated by reverse mutation of the amino acid residues. Luciferase activity assay was used to assess the transduction efficiency of the reverted mutants related to hybrid capsids: (D) AAV2-2208, (E) AAV2-2128, and (F) AAV2-2141. The corresponding WT AAV variant of each hybrid capsid was tested in parallel as control. Horizontal dotted line indicates the luciferase activity level of AAV2 reference capsid. Statistical analysis was performed using one-way ANOVA with Dunnett's multiple comparisons test. The corresponding WT AAV variant was used as control group for mean comparison. $*p < 0.05$, $**p < 0.01$, $***p < 0.001$, $****p < 0.0001$.

the AAV2 capsid that were shown to yield an antibody-evading phenotype.[33] The manuscript did not detail all the sequences but allowed us to retrieve 41 capsid sequences derived from the original pool prior to selection and 43 sequences identified after the screening, which were likely viable (Figure 6A). The minimum s' score per variant was calculated to predict the viability of each capsid. Of note, while capsids before selection ($n = 41$) had a variable s' score, selected mutants, produced and thus considered as viable ($n = 43$), invariably had a high s' score (Figure S11A). The second collection of capsids comprised mutants generated by site-directed mutagenesis at 59 different positions in the AAV2 capsid.[34] We retrieved the sequences of 46 capsids with multiple point mutations (Figure 6A) that the authors grouped into four classes based on infectious titer assay: class 1 containing mutants with infectious titer similar to the WT titer, class 2 containing partially defective mutants with infectious titers 2 to 3 logs lower than the WT titer, class 3 including temperature-sensitive mutants, and class 4 consisting of non-infectious mutants with titers more than 5 logs lower than the parental capsid. In line with this classification, our s' score analysis revealed progressively decreased s' values from class 1 to class 4 (Figure S11B). We considered mutants of class 1 and 2 as viable, and class 4 as non-viable. Class 3 was excluded given the low number of components ($n = 3$) and the difficulty in interpreting the temperature-sensitive character of a capsid in terms of viability.

Altogether, we used 74 viable and 12 non-viable variants to validate our prediction method (Figure 6B). Our analysis of the s' scores enabled the accurate prediction of 99% of mutants. These findings further support the hypothesis that the independence of the mutations can serve as a reliable means for predicting the viability of capsids with multiple amino acid variations along the VP, as demonstrated by the receiver operating characteristic (ROC) curve analysis on our capsids' series and on the public dataset (Figure 6C).

Our prediction method tested on a total of 135 variants (49 from our cohort and 86 publicly available) allowed to infer AAV2 capsid viability with a sensitivity of 98%, an accuracy of 98%, and a specificity of 95% (Figures S11C and S11D).

DISCUSSION

In this study, we assessed the viability of 56 novel capsid variants recently isolated from human liver tissues[23] and we investigated the profile of their mutations in depth. Integration of our data with the dataset from Ogden and colleagues[4] allowed to clearly pinpoint deleterious mutations and to develop an approach to easily predict viability in capsids bearing multiple mutations, relying on the s' scores of individual mutations.

In total, 71% of the variants were successfully produced, able to transduce cells and, consequently, classified as viable. Concerning the non-viable variants ($n = 16$), we identified the presence of heterogeneous

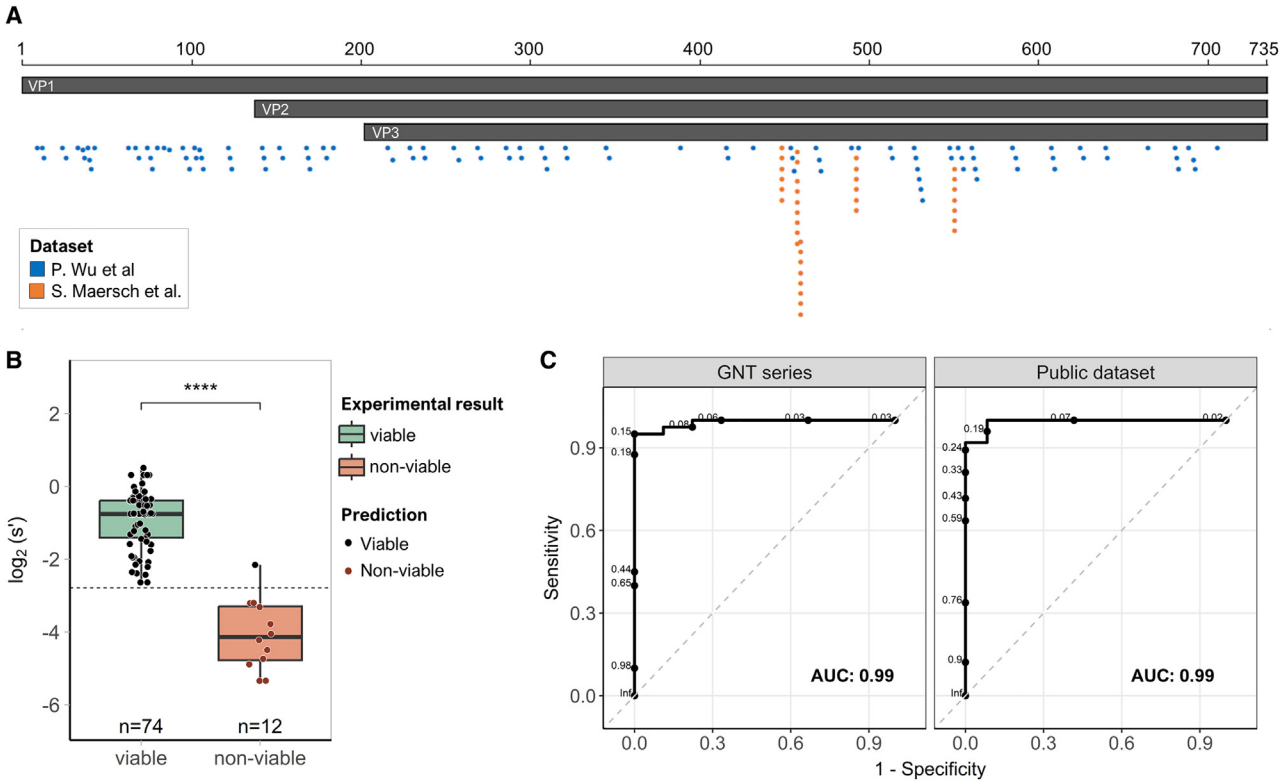

Figure 6. Validation of the prediction method on public datasets

(A) Schematic representation of AAV2 capsid amino acid sequences with mutations described in two independent public datasets.[33,34] (B) Median s' score in viable and non-viable capsids classified according to experimental data. Each point represents the lowest s' (s'_{min}) value among all mutations of a capsid to underline the presence of deleterious mutations in the sequence. Statistical analysis was performed using Wilcoxon rank-sum test. (C) ROC curves representing the performance of the prediction method in the collection of WT variants (GNT series) and in public datasets. *$p < 0.05$, **$p < 0.01$, ***$p < 0.001$, ****$p < 0.0001$.

indels in terms of size and localization in six variants, and a frameshift mutation in one variant that might have destabilized the capsid structure. However, when we analyzed both structural and non-structural proteins, we found no common mutations or hotspots of deleterious amino acid change. Based on this observation, we hypothesized that unique mutations, specific to each variant, were negatively affecting capsid viability.

Single amino acid mutations in VP sequence have been described to impact multiple capsid properties, including viability, tropism, transduction efficiency, and immunogenicity.[4,16,35–37] In 2019, Ogden and colleagues performed the most extensive characterization of the role of single amino acid mutations on AAV2 capsid viability and tropism.[4] Each single mutation was associated with a fitness score reflecting the impact of the mutation on capsid production compared with AAV2 reference. Leveraging this dataset, we conducted viability analysis on our variants, assuming the independent impact of each mutation on the capsid viability of a variant. The analysis of the s' score distribution in common and unique mutations revealed a clear distinct profile highlighting a group of unique mutations at low s' score, which we considered as potentially deleterious. Based on this pattern, we defined a fitness score threshold for deleterious mutations and predicted capsid viability assuming that non-viable capsids were those having one or more mutations below that threshold. To test our hypothesis, some potential deleterious mutations were experimentally validated proving their clear impact on capsid viability. Interestingly, the 15 potentially deleterious mutations identified in our variants are not present in any other analyzed AAV serotypes, suggesting that these mutations may be deleterious regardless of the AAV capsid serotype. The presence of deleterious mutations in WT variants was unexpected, although not entirely surprising, given the rapid kinetics of AAV capsid mutation during replication.[26] This phenomenon, described as an adaptation mechanism, occurs both *in vitro* and *in vivo*. It is plausible that deleterious mutations emerged over time during replication in the human liver. Furthermore, considering that the biological environment and selective pressures encountered by viruses and vector can be significantly different, we cannot exclude the possibility that these mutations may exert different effects in a viral context compared with a vector context.

The prediction method was tested on our own variants and validated on external datasets allowing to infer AAV2 capsid viability with 98% sensitivity, 98% accuracy, and 95% specificity. Noteworthy, the predicted variants were characterized by the presence of multiple

mutations along the VP sequence, whereas the fitness score was associated with capsids bearing individual mutations, suggesting that the data related to single mutations can be used to predict the viability within the context of multiple mutations. These results strongly support our hypothesis of mutations independence, which implies that capsid viability is determined by the independent impacts of single mutations and not by their cumulative effect. In line with this hypothesis, we observed that the presence of mutations with a high s' score cannot compensate the irreversible impairment caused by a single deleterious amino acid change, suggesting that a positive epistatic effect of mutations is unlikely to occur. The mutation independence hypothesis aligns with the work performed by Ogden and colleagues, highlighting the potential of systematic mutagenesis in unraveling complex genomes.

The mutation fitness was analyzed according to four different parameters to identify common features that might influence mutation outcomes. Two parameters were related to the 3D position of the mutated residues, accessibility in the capsid and HVR localization, and two were strictly related to the type of mutation, changes in hydrophobicity and polarity of lateral chains of the amino acids. Notably, the accessibility of residues within the 3D structure of the 60-mer AAV capsid and the HVR localization emerged as the key parameters affecting capsid viability. It was observed that mutations of residues in buried regions were more frequently deleterious than mutations of residues in accessible regions. This finding suggests that the localization of the mutation plays a more significant role than the specific type of variation when predicting capsid viability. Buried residues are indeed more conserved among different AAV serotypes, indicating their structural importance in stabilizing the capsid.[7,38] Consequently, residues located in accessible regions, mostly represented by HVRs, were more prompt to tolerate mutations than residues in buried regions. We investigated the interplay between residue accessibility and HVR localization in predicting the fitness of the mutations and showed that 64% of mutations occurring in buried regions outside HVRs were deleterious compared with only 14% of mutations in accessible region within HVRs.

HVRs are a common target of capsid engineering due to their localization in exposed domains and their crucial role in the interaction with host cell receptors.[21,22,39,40] Even though the residues within these regions are mostly exposed, 44% of the amino acids composing the HVRs are buried in an assembled capsid (data from AAV2, PDB: 1LP3). Noteworthy, 3 out of 15 deleterious mutations in our non-viable capsids were located in buried positions within HVRs. Our findings underscore the importance of careful assessment of residue accessibility when designing novel engineered capsids, especially when employing random mutagenesis approaches to enhance capsid diversity, even if the target region is HVR.

Different capsid engineering strategies have been developed and used over the years to improve the transduction efficiency and tailor the tissue specificity of the capsids.[20] The most popular approach is directed evolution which involves the generation of a library composed of millions of variants followed by iterative rounds of selection to identify the best candidates for a specific capsid feature. These libraries can be generated through different techniques, such as error-prone PCR or capsid shuffling, which do not require any previous knowledge on capsid structure and sequences. These approaches allow to easily generate large variant libraries with a potential high rate of capsid diversity. However, several studies have shown that these libraries often contain a substantial proportion of non-viable capsids.[4,21,22] The lack of knowledge on capsid structure and on the consequences of amino acid mutations represent a significant challenge in capsid engineering. The advent of bioinformatics and machine learning in the gene therapy field is aiding to tackle this gap but, at this stage, these approaches require large empirical datasets to predict capsids features, such as viability or tropism.[4,21,40,41] In this context, the study of WT capsids might help to identify regions that are more tolerant of mutations, thereby implementing our understanding of capsid structure and stability.

The investigation on WT AAV2 variants in our study has shed light on common features associated with amino acid residues posing high risk to capsid viability. This knowledge, when integrated into the design of novel AAV libraries may reduce the frequency of non-viable capsids. Furthermore, our results provide strong support for the value of characterizing libraries created through systematic single mutagenesis of the VP sequence as a unique resource to predict the viability of capsids with multiple variations. To conclude, the analysis model developed in this work might be useful to guide future designs of AAV libraries enriched in viable capsids and to accelerate the identification of therapeutic candidates among engineered capsids.

MATERIALS AND METHODS

Capsid sequences and phylogenetic analysis

Capsids variants from AAV2 (n = 25) and AAV2-13 (n = 34) genotypes were previously isolated from human liver.[23] Consensus sequences of AAV2 and AAV2-13 genotypes were obtained by multiple sequence alignment (MSA) using MultiAlin software.[42] The consensus sequences were used to remove ambiguous nucleotide positions present in some capsid sequences deposited in GenBank database. In this case, ambiguous nucleotides were substituted with the corresponding nucleotide of the consensus sequences of the same AAV genotype.

To remove redundant amino acid sequences, a pairwise analysis on MSA of all AAV variants was performed using MEGA X.[43] Evolutionary divergence was estimated in terms of the number of amino acid differences between each couple of sequences. All sequences containing at least one amino acid of difference in the pairwise matrix were selected for further analysis.

Phylogenetic analysis on amino acid VP sequences were performed using MEGA X.[43] The evolutionary history was inferred using the neighbor joining method.[27] Poisson correction method was used to compute the evolutionary distances[28] in the units of the number of

amino acid substitutions per site. All ambiguous positions were removed for each sequence pair (pairwise deletion option).

Cloning of the capsid sequences

The pRep2Cap2 plasmid, encoding for Rep and Cap proteins of AAV2, was used as backbone plasmid to clone both WT and mutated hybrid capsids.

The Cap sequence of AAV2 in pRep2Cap2 plasmid was replaced with the newly synthetized capsid sequences of WT AAV variants.

To validate deleterious mutations, hybrid AAV2 capsids were generated by modification of a 256 amino acid region spanning from positions 350 to 606 of the Cap sequence of the pRep2Cap2 plasmid. This region was substituted with the corresponding region of non-viable capsids #2141, #2128, and #2208 to generate hybrid AAV capsids. Potentially deleterious mutations in hybrid capsids were reverted to AAV2 sequence by site-directed mutagenesis.

All plasmids were manufactured by Genecust, which performed sequence synthesis, cloning, and site-directed mutagenesis.

AAV vector production

AAV vectors were produced by an adenovirus-free transient triple transfection method of HEK293T cells in suspension with proprietary modified cells and protocol. In brief, 50 mL HEK293T cell growing in agitation in shake flasks was transfected with the three plasmids containing the adenovirus helper proteins, the AAV Rep and Cap genes, and the inverted terminal repeat-flanked transgene expression cassette (firefly luciferase reporter gene under the control of a CMV promoter). After 24 h of transfection, cells were treated by Benzonase (Merck-Millipore). Seventy-two hours post transfection cells were lysed by Triton X-100 (Sigma-Aldrich), the cell culture was centrifuged, and supernatant was collected. Vectors were purified by affinity chromatography using ÄKTA pure (Cytiva). The final product was formulated in sterile PBS containing 0.001% of Pluronic (Sigma-Aldrich) and stored at −80°C.

Vector DNA before and after purification was extracted using MagNA Pure 96 DNA and a Viral NA Small Volume Kit (Roche) following the manufacturer's protocol. AAV vector titration was performed by real-time quantitative PCR using LightCycler 480 System (Roche). Final titers were expressed as vg/mL.

Cell culture and luciferase assay

2V6.11 cells (catalog no. CRL-2784; ATCC) were maintained at 37°C and 5% CO_2 in DMEM supplemented with 10% FCS and 2 mM of GlutaMAX (Gibco). Cells were transduced with AAV vectors at 10,000 multiplicity of infection and luciferase assay was performed after 48 h using the Britelite plus Reporter Gene Assay System (PerkinElmer). Luciferase activity was measured at EnSpire (PerkinElmer) in a white opaque 96-well plate. Relative luminescence unit value of transduced cell was normalized on the background signal of non-transduced cells.

To test the luciferase activity of bulk AAV production, AAV vectors were collected from the medium through lysis of producer cells followed by centrifugation at 1,000 × *g* for 10 min at RT. Supernatants were collected and *in vitro* transduction efficiency was tested. 2V6.11 cells were transduced with vectors from bulk production and luciferase assay was performed 48 h later, as described previously.

3D structure analysis

3D structures of full AAV2 (PDB: 1LP3) and AAV13 (PDB: 7L6H) capsids available on RCSB Protein DataBank (RCSB PDB) were analyzed using Mol* Viewer.[44] The VP monomers of AAV2 and AAV13 capsids were superimposed, and the RMSD was calculated. Information related to residue accessibility (classification in buried and accessible amino acids) and accessible surface area of each amino acid were directly extracted from PDB files. The percentage of accessible surface area was calculated by dividing the accessible surface area of each residue by the total surface area of the amino acids empirically determined by Tien and colleagues.[45]

The 3D structures of non-viable capsids with frameshift mutation and indels were predicted using ColabFold (version 1.5.2) based on AlphaFold2 and MMseqs2 for structure prediction and sequence alignment, respectively.[46] Predicted structures were superimposed to the AAV13 VP monomer using Mol* Viewer and the RMSD values were calculated.

All 3D structure representations were generated using Mol* Viewer.[44]

Calculation of GRAVY index

To investigate the possible change in hydrophobicity due to indels and frameshift mutation in the capsid, the GRAVY index of the protein regions impacted by the mutations was analyzed. The GRAVY score of mutated regions and the corresponding WT AAV13 regions was computed using the ProtParam tool on the ExPASy server.

Statistical analysis

Statistical analyses were performed using RStudio (R version 4.2.2) and GraphPad Prism (version 9.3.1). Statistical significance of quantitative variable was determined by Wilcoxon rank-sum test. The frequency of mutations according to different parameters (variation in hydrophobicity, classification according to s' score, localization in the VP sequence) was investigated using χ^2 test. Adjustment of *p* values was computed for a Monte Carlo test with 2,000 permutations.

Fitting generalized linear model was used to assess the contribution of residue features in predicting the outcome of a mutation (neutral versus deleterious). This analysis was performed using the glm function included in the stats package in R.

Luciferase activity and production yield (vg/mL) of cells transduced with AAV variants or mutants versus transduced control cells were compared using one-way ANOVA with Dunnett's multiple comparisons test.

The modality of the distributions was assessed by Hartigan's dip test for unimodality/multimodality with simulated p value (based on 2,000 replicates). p values less than 0.05 indicate significant multimodality, whereas p values greater than 0.05 but less than 0.10 suggest multimodality with marginal significance.[47] When H_0 for normal distribution was rejected, alternative hypothesis of multimodality was validated by LaplacesDemon package's functions in R.

ROC and precision-recall curves were used to evaluate the performance of the prediction model at all s' thresholds. PlotROC and precrec package's functions in R were used to generate the curves and calculate the corresponding area under the curve.

A detailed description of the prediction model and its validation is available in the supplemental information.

DATA AND CODE AVAILABILITY

The authors confirm that the data supporting the findings of this study are available within the article and its supplemental materials. All requests for raw and analyzed data and materials are available upon reasonable request, Giuseppe Ronzitti (gronzitti@genethon.fr).

ACKNOWLEDGMENTS

This work was supported by Genethon. T.L.B., B.B., A.M., J.N., and P.V. are Genopole's members, first French biocluster dedicated to genetics, biotechnologies, and biotherapies. A.M.'s salary was covered by a Eurostars grant (E115712 – AAVanguard). We are grateful to Ile-de-France Region, to Conseil Départemental de l'Essonne (ASTRE), to "Institut National de la Santé et de la Recherche Médicale" (Inserm), and GIP Genopole, Evry, for the purchase of the equipment.

AUTHOR CONTRIBUTIONS

T.L.B., B.B., A.M., J.N., and P.V. were involved in the generation of experimental data. T.L.B. and G.R. analyzed and interpreted the data. T.L.B., S.I., J.-C.N., and J.Z.-R. were involved in the isolation of AAV variants and the initial analysis. T.L.B. and G.R. wrote the manuscript. All authors provided review and editing of the manuscript.

DECLARATION OF INTERESTS

T.L.B., P.V., J.N., G.R., S.I., J.-C.N., and J.Z.-R. are authors in patents related to capsids development. G.R. is associate editor of the journal *Molecular Therapy Methods & Clinical Development*.

SUPPLEMENTAL INFORMATION

Supplemental information can be found online at https://doi.org/10.1016/j.omtm.2024.101327.

REFERENCES

1. Atchison, R.W., Casto, B.C., and Hammon, W.M. (1965). Adenovirus-Associated Defective Virus Particles. Science *149*, 754–756. https://doi.org/10.1126/science.149.3685.754.

2. Balakrishnan, B., and Jayandharan, G.R. (2014). Basic biology of adeno-associated virus (AAV) vectors used in gene therapy. Curr. Gene Ther. *14*, 86–100. https://doi.org/10.2174/1566523214666140302193709.

3. Cao, M., You, H., and Hermonat, P.L. (2014). The X gene of adeno-associated virus 2 (AAV2) is involved in viral DNA replication. PLoS One *9*, e104596. https://doi.org/10.1371/journal.pone.0104596.

4. Ogden, P.J., Kelsic, E.D., Sinai, S., and Church, G.M. (2019). Comprehensive AAV capsid fitness landscape reveals a viral gene and enables machine-guided design. Science *366*, 1139–1143. https://doi.org/10.1126/science.aaw2900.

5. Sonntag, F., Schmidt, K., and Kleinschmidt, J.A. (2010). A viral assembly factor promotes AAV2 capsid formation in the nucleolus. Proc. Natl. Acad. Sci. USA *107*, 10220–10225. https://doi.org/10.1073/pnas.1001673107.

6. Stutika, C., Gogol-Döring, A., Botschen, L., Mietzsch, M., Weger, S., Feldkamp, M., Chen, W., and Heilbronn, R. (2016). A Comprehensive RNA Sequencing Analysis of the Adeno-Associated Virus (AAV) Type 2 Transcriptome Reveals Novel AAV Transcripts, Splice Variants, and Derived Proteins. J. Virol. *90*, 1278–1289. https://doi.org/10.1128/JVI.02750-15.

7. Gao, G., Alvira, M.R., Somanathan, S., Lu, Y., Vandenberghe, L.H., Rux, J.J., Calcedo, R., Sanmiguel, J., Abbas, Z., and Wilson, J.M. (2003). Adeno-associated viruses undergo substantial evolution in primates during natural infections. Proc. Natl. Acad. Sci. USA *100*, 6081–6086. https://doi.org/10.1073/pnas.0937739100.

8. Colella, P., Ronzitti, G., and Mingozzi, F. (2018). Emerging Issues in AAV-Mediated In Vivo Gene Therapy. Mol. Ther. Methods Clin. Dev. *8*, 87–104. https://doi.org/10.1016/j.omtm.2017.11.007.

9. George, L.A., Monahan, P.E., Eyster, M.E., Sullivan, S.K., Ragni, M.V., Croteau, S.E., Rasko, J.E.J., Recht, M., Samelson-Jones, B.J., MacDougall, A., et al. (2021). Multiyear Factor VIII Expression after AAV Gene Transfer for Hemophilia A. N. Engl. J. Med. *385*, 1961–1973. https://doi.org/10.1056/NEJMoa2104205.

10. Kuzmin, D.A., Shutova, M.V., Johnston, N.R., Smith, O.P., Fedorin, V.V., Kukushkin, Y.S., van der Loo, J.C.M., and Johnstone, E.C. (2021). The clinical landscape for AAV gene therapies. Nat. Rev. Drug Discov. *20*, 173–174. https://doi.org/10.1038/d41573-021-00017-7.

11. Gao, G., Vandenberghe, L.H., Alvira, M.R., Lu, Y., Calcedo, R., Zhou, X., and Wilson, J.M. (2004). Clades of Adeno-associated viruses are widely disseminated in human tissues. J. Virol. *78*, 6381–6388. https://doi.org/10.1128/JVI.78.12.6381-6388.2004.

12. Gao, G.P., Alvira, M.R., Wang, L., Calcedo, R., Johnston, J., and Wilson, J.M. (2002). Novel adeno-associated viruses from rhesus monkeys as vectors for human gene therapy. Proc. Natl. Acad. Sci. USA *99*, 11854–11859. https://doi.org/10.1073/pnas.182412299.

13. Mori, S., Wang, L., Takeuchi, T., and Kanda, T. (2004). Two novel adeno-associated viruses from cynomolgus monkey: pseudotyping characterization of capsid protein. Virology *330*, 375–383. https://doi.org/10.1016/j.virol.2004.10.012.

14. Schmidt, M., Govindasamy, L., Afione, S., Kaludov, N., Agbandje-McKenna, M., and Chiorini, J.A. (2008). Molecular characterization of the heparin-dependent transduction domain on the capsid of a novel adeno-associated virus isolate, AAV(VR-942). J. Virol. *82*, 8911–8916. https://doi.org/10.1128/JVI.00672-08.

15. Schmidt, M., Voutetakis, A., Afione, S., Zheng, C., Mandikian, D., and Chiorini, J.A. (2008). Adeno-associated virus type 12 (AAV12): a novel AAV serotype with sialic acid- and heparan sulfate proteoglycan-independent transduction activity. J. Virol. *82*, 1399–1406. https://doi.org/10.1128/JVI.02012-07.

16. Emmanuel, S.N., Smith, J.K., Hsi, J., Tseng, Y.S., Kaplan, M., Mietzsch, M., Chipman, P., Asokan, A., McKenna, R., and Agbandje-McKenna, M. (2022). Structurally Mapping Antigenic Epitopes of Adeno-associated Virus 9: Development of Antibody Escape Variants. J. Virol. *96*, e0125121. https://doi.org/10.1128/JVI.01251-21.

17. Puzzo, F., Zhang, C., Powell Gray, B., Zhang, F., Sullenger, B.A., and Kay, M.A. (2023). Aptamer-programmable adeno-associated viral vectors as a novel platform for cell-specific gene transfer. Mol. Ther. Nucleic Acids *31*, 383–397. https://doi.org/10.1016/j.omtn.2023.01.007.

18. Weinmann, J., Weis, S., Sippel, J., Tulalamba, W., Remes, A., El Andari, J., Herrmann, A.K., Pham, Q.H., Borowski, C., Hille, S., et al. (2020). Identification of a myotropic AAV by massively parallel in vivo evaluation of barcoded capsid variants. Nat. Commun. *11*, 5432. https://doi.org/10.1038/s41467-020-19230-w.

19. Zhang, L., Rossi, A., Lange, L., Meumann, N., Koitzsch, U., Christie, K., Nesbit, M.A., Moore, C.B.T., Hacker, U.T., Morgan, M., et al. (2019). Capsid Engineering Overcomes Barriers Toward Adeno-Associated Virus Vector-Mediated Transduction of Endothelial Cells. Hum. Gene Ther. *30*, 1284–1296. https://doi.org/10.1089/hum.2019.027.

20. Wang, D., Tai, P.W.L., and Gao, G. (2019). Adeno-associated virus vector as a platform for gene therapy delivery. Nat. Rev. Drug Discov. *18*, 358–378. https://doi.org/10.1038/s41573-019-0012-9.

21. Han, Z., Luo, N., Wang, F., Cai, Y., Yang, X., Feng, W., Zhu, Z., Wang, J., Wu, Y., Ye, C., et al. (2023). Computer-Aided Directed Evolution Generates Novel AAV Variants with High Transduction Efficiency. Viruses *15*, 848. https://doi.org/10.3390/v15040848.

22. Marsic, D., Govindasamy, L., Currlin, S., Markusic, D.M., Tseng, Y.S., Herzog, R.W., Agbandje-McKenna, M., and Zolotukhin, S. (2014). Vector design Tour de Force: integrating combinatorial and rational approaches to derive novel adeno-associated virus variants. Mol. Ther. *22*, 1900–1909. https://doi.org/10.1038/mt.2014.139.

23. La Bella, T., Imbeaud, S., Peneau, C., Mami, I., Datta, S., Bayard, Q., Caruso, S., Hirsch, T.Z., Calderaro, J., Morcrette, G., et al. (2020). Adeno-associated virus in the liver: natural history and consequences in tumour development. Gut *69*, 737–747. https://doi.org/10.1136/gutjnl-2019-318281.

24. Meliani, A., Leborgne, C., Triffault, S., Jeanson-Leh, L., Veron, P., and Mingozzi, F. (2015). Determination of anti-adeno-associated virus vector neutralizing antibody titer with an in vitro reporter system. Hum. Gene Ther. Methods *26*, 45–53. https://doi.org/10.1089/hgtb.2015.037.

25. Ellis, B.L., Hirsch, M.L., Barker, J.C., Connelly, J.P., Steininger, R.J., 3rd, and Porteus, M.H. (2013). A survey of ex vivo/in vitro transduction efficiency of mammalian primary cells and cell lines with Nine natural adeno-associated virus (AAV1-9) and one engineered adeno-associated virus serotype. Virol. J. *10*, 74. https://doi.org/10.1186/1743-422X-10-74.

26. Cabanes-Creus, M., Hallwirth, C.V., Westhaus, A., Ng, B.H., Liao, S.H.Y., Zhu, E., Navarro, R.G., Baltazar, G., Drouyer, M., Scott, S., et al. (2020). Restoring the natural tropism of AAV2 vectors for human liver. Sci. Transl. Med. *12*, eaba3312. https://doi.org/10.1126/scitranslmed.aba3312.

27. Saitou, N., and Nei, M. (1987). The neighbor-joining method: a new method for reconstructing phylogenetic trees. Mol. Biol. Evol. *4*, 406–425. https://doi.org/10.1093/oxfordjournals.molbev.a040454.

28. Zuckerkandl, E., and Pauling, L. (1965). Evolutionary divergence and convergence in proteins. In Evolving Genes and Proteins, V. Bryson and H.J. Vogel, eds. (Academic Press).

29. Kyte, J., and Doolittle, R.F. (1982). A simple method for displaying the hydropathic character of a protein. J. Mol. Biol. *157*, 105–132. https://doi.org/10.1016/0022-2836(82)90515-0.

30. Borner, K., Kienle, E., Huang, L.Y., Weinmann, J., Sacher, A., Bayer, P., Stullein, C., Fakhiri, J., Zimmermann, L., Westhaus, A., et al. (2020). Pre-arrayed Pan-AAV Peptide Display Libraries for Rapid Single-Round Screening. Mol. Ther. *28*, 1016–1032. https://doi.org/10.1016/j.ymthe.2020.02.009.

31. Dalkara, D., Byrne, L.C., Klimczak, R.R., Visel, M., Yin, L., Merigan, W.H., Flannery, J.G., and Schaffer, D.V. (2013). In vivo-directed evolution of a new adeno-associated virus for therapeutic outer retinal gene delivery from the vitreous. Sci. Transl. Med. *5*, 189ra76. https://doi.org/10.1126/scitranslmed.3005708.

32. Perabo, L., Büning, H., Kofler, D.M., Ried, M.U., Girod, A., Wendtner, C.M., Enssle, J., and Hallek, M. (2003). In vitro selection of viral vectors with modified tropism: the adeno-associated virus display. Mol. Ther. *8*, 151–157. https://doi.org/10.1016/s1525-0016(03)00123-0.

33. Maersch, S., Huber, A., Büning, H., Hallek, M., and Perabo, L. (2010). Optimization of stealth adeno-associated virus vectors by randomization of immunogenic epitopes. Virology *397*, 167–175. https://doi.org/10.1016/j.virol.2009.10.021.

34. Wu, P., Xiao, W., Conlon, T., Hughes, J., Agbandje-McKenna, M., Ferkol, T., Flotte, T., and Muzyczka, N. (2000). Mutational analysis of the adeno-associated virus type 2 (AAV2) capsid gene and construction of AAV2 vectors with altered tropism. J. Virol. *74*, 8635–8647. https://doi.org/10.1128/jvi.74.18.8635-8647.2000.

35. Cabanes-Creus, M., Westhaus, A., Navarro, R.G., Baltazar, G., Zhu, E., Amaya, A.K., Liao, S.H.Y., Scott, S., Sallard, E., Dilworth, K.L., et al. (2020). Attenuation of Heparan Sulfate Proteoglycan Binding Enhances In Vivo Transduction of Human Primary Hepatocytes with AAV2. Mol. Ther. Methods Clin. Dev. *17*, 1139–1154. https://doi.org/10.1016/j.omtm.2020.05.004.

36. Crosson, S.M., Bennett, A., Fajardo, D., Peterson, J.J., Zhang, H., Li, W., Leahy, M.T., Jennings, C.K., Boyd, R.F., Boye, S.L., et al. (2021). Effects of Altering HSPG Binding and Capsid Hydrophilicity on Retinal Transduction by AAV. J. Virol. *95*, e02440-20. https://doi.org/10.1128/JVI.02440-20.

37. Cabanes-Creus, M., Navarro, R.G., Liao, S.H.Y., Baltazar, G., Drouyer, M., Zhu, E., Scott, S., Luong, C., Wilson, L.O.W., Alexander, I.E., and Lisowski, L. (2021). Single amino acid insertion allows functional transduction of murine hepatocytes with human liver tropic AAV capsids. Mol. Ther. Methods Clin. Dev. *21*, 607–620. https://doi.org/10.1016/j.omtm.2021.04.010.

38. Rayaprolu, V., Kruse, S., Kant, R., Venkatakrishnan, B., Movahed, N., Brooke, D., Lins, B., Bennett, A., Potter, T., McKenna, R., et al. (2013). Comparative analysis of adeno-associated virus capsid stability and dynamics. J. Virol. *87*, 13150–13160. https://doi.org/10.1128/JVI.01415-13.

39. Biswas, M., Marsic, D., Li, N., Zou, C., Gonzalez-Aseguinolaza, G., Zolotukhin, I., Kumar, S.R.P., Rana, J., Butterfield, J.S.S., Kondratov, O., et al. (2020). Engineering and In Vitro Selection of a Novel AAV3B Variant with High Hepatocyte Tropism and Reduced Seroreactivity. Mol. Ther. Methods Clin. Dev. *19*, 347–361. https://doi.org/10.1016/j.omtm.2020.09.019.

40. Bryant, D.H., Bashir, A., Sinai, S., Jain, N.K., Ogden, P.J., Riley, P.F., Church, G.M., Colwell, L.J., and Kelsic, E.D. (2021). Deep diversification of an AAV capsid protein by machine learning. Nat. Biotechnol. *39*, 691–696. https://doi.org/10.1038/s41587-020-00793-4.

41. Marques, A.D., Kummer, M., Kondratov, O., Banerjee, A., Moskalenko, O., and Zolotukhin, S. (2021). Applying machine learning to predict viral assembly for adeno-associated virus capsid libraries. Mol. Ther. Methods Clin. Dev. *20*, 276–286. https://doi.org/10.1016/j.omtm.2020.11.017.

42. Corpet, F. (1988). Multiple sequence alignment with hierarchical clustering. Nucleic Acids Res. *16*, 10881–10890. https://doi.org/10.1093/nar/16.22.10881.

43. Kumar, S., Stecher, G., Li, M., Knyaz, C., and Tamura, K. (2018). MEGA X: Molecular Evolutionary Genetics Analysis across Computing Platforms. Mol. Biol. Evol. *35*, 1547–1549. https://doi.org/10.1093/molbev/msy096.

44. Sehnal, D., Bittrich, S., Deshpande, M., Svobodová, R., Berka, K., Bazgier, V., Velankar, S., Burley, S.K., Koča, J., and Rose, A.S. (2021). Mol* Viewer: modern web app for 3D visualization and analysis of large biomolecular structures. Nucleic Acids Res. *49*, W431–W437. https://doi.org/10.1093/nar/gkab314.

45. Tien, M.Z., Meyer, A.G., Sydykova, D.K., Spielman, S.J., and Wilke, C.O. (2013). Maximum allowed solvent accessibilites of residues in proteins. PLoS One *8*, e80635. https://doi.org/10.1371/journal.pone.0080635.

46. Mirdita, M., Schütze, K., Moriwaki, Y., Heo, L., Ovchinnikov, S., and Steinegger, M. (2022). ColabFold: making protein folding accessible to all. Nat. Methods *19*, 679–682. https://doi.org/10.1038/s41592-022-01488-1.

47. Freeman, J.B., and Dale, R. (2013). Assessing bimodality to detect the presence of a dual cognitive process. Behav. Res. Methods *45*, 83–97. https://doi.org/10.3758/s13428-012-0225-x.